Article

Cell Reports

Metabolically Activated Adipose Tissue Macrophages Perform Detrimental and Beneficial Functions during Diet-Induced Obesity

Graphical Abstract

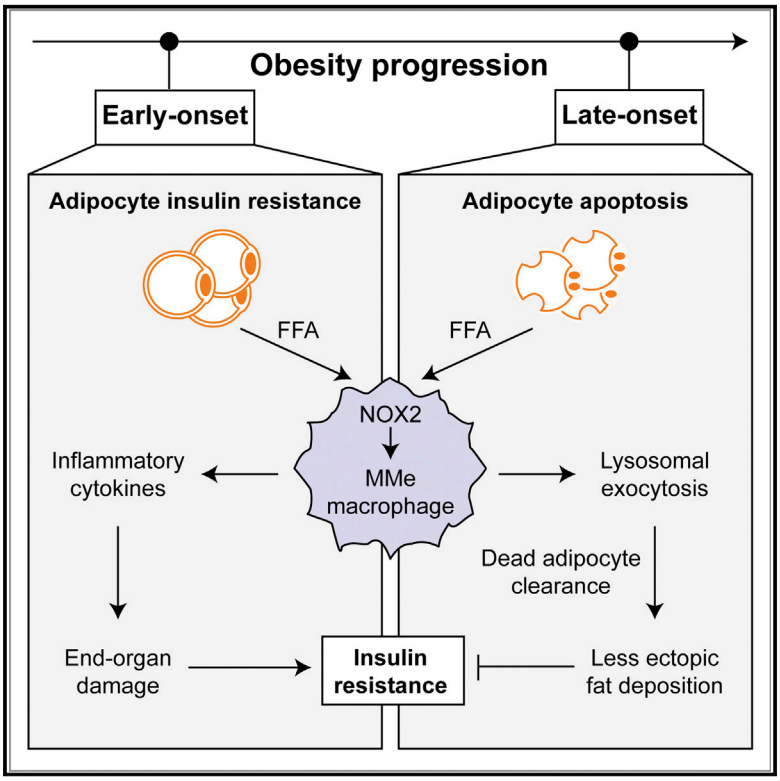

Highlights

- Inflammation and dead adipocyte clearance by MMe macrophages require NOX2
- *Nox2*$^{-/-}$ improves the metabolic phenotype in early DIO but worsens it in late DIO
- Early improvements associate with suppressed ATM inflammation
- Late worsening associates with lower ATM lysosomal exocytosis to dead adipocytes

Authors

Brittney R. Coats, Kelly Q. Schoenfelt, Valéria C. Barbosa-Lorenzi, ..., Christopher J. Rhodes, Frederick R. Maxfield, Lev Becker

Correspondence

levb@uchicago.edu

In Brief

During obesity, adipose tissue macrophages are metabolically activated (MMe). Coats et al. show that MMe macrophages perform detrimental (potentiate inflammation) and beneficial (exocytose lysosomes to clear dead adipocytes) functions, controlled by NOX2. *Nox2*$^{-/-}$ mice exhibit improved or worsened metabolic phenotypes depending on high-fat-diet duration, highlighting the dynamic contributions of MMe macrophages in obesity.

Coats et al., 2017, Cell Reports *20*, 3149–3161
September 26, 2017
http://dx.doi.org/10.1016/j.celrep.2017.08.096

Cell Reports
Article

Metabolically Activated Adipose Tissue Macrophages Perform Detrimental and Beneficial Functions during Diet-Induced Obesity

Brittney R. Coats,[1,5] Kelly Q. Schoenfelt,[2,5] Valéria C. Barbosa-Lorenzi,[3,5] Eduard Peris,[1] Chang Cui,[2] Alexandria Hoffman,[1] Guolin Zhou,[2] Sully Fernandez,[1] Lijie Zhai,[1] Ben A. Hall,[1] Abigail S. Haka,[3] Ajay M. Shah,[4] Catherine A. Reardon,[1,2] Matthew J. Brady,[1] Christopher J. Rhodes,[1] Frederick R. Maxfield,[3] and Lev Becker[1,2,6,*]
[1]Committee on Molecular Metabolism and Nutrition
[2]Ben May Department for Cancer Research
The University of Chicago, Chicago, IL 60637, USA
[3]Department of Biochemistry, Weill Cornell Medical College, New York, NY 10065, USA
[4]Cardiovascular Division, King's College, London British Hearth Foundation Centre, London SE5 9NU, UK
[5]These authors contributed equally
[6]Lead Contact
*Correspondence: levb@uchicago.edu
http://dx.doi.org/10.1016/j.celrep.2017.08.096

SUMMARY

During obesity, adipose tissue macrophages (ATMs) adopt a metabolically activated (MMe) phenotype. However, the functions of MMe macrophages are poorly understood. Here, we combine proteomic and functional methods to demonstrate that, in addition to potentiating inflammation, MMe macrophages promote dead adipocyte clearance through lysosomal exocytosis. We identify NADPH oxidase 2 (NOX2) as a driver of the inflammatory and adipocyte-clearing properties of MMe macrophages and show that, compared to wild-type, *Nox2*$^{-/-}$ mice exhibit a time-dependent metabolic phenotype during diet-induced obesity. After 8 weeks of high-fat feeding, *Nox2*$^{-/-}$ mice exhibit attenuated ATM inflammation and mildly improved glucose tolerance. After 16 weeks of high-fat feeding, *Nox2*$^{-/-}$ mice develop severe insulin resistance, hepatosteatosis, and visceral lipoatrophy characterized by dead adipocyte accumulation and defective ATM lysosomal exocytosis, a phenotype reproduced in myeloid cell-specific *Nox2*$^{-/-}$ mice. Collectively, our findings suggest that MMe macrophages perform detrimental and beneficial functions whose contribution to metabolic phenotypes during obesity is determined by disease progression.

INTRODUCTION

During obesity, macrophages accumulate in visceral adipose tissue, where they promote chronic low-grade inflammation (Weisberg et al., 2003; Xu et al., 2003). It is well accepted that this inflammation is causally associated with insulin resistance in mice. Inhibiting several pathways that drive inflammatory signaling and/or production in macrophages improves insulin sensitivity during obesity (Han et al., 2013; Patsouris et al., 2008; Saberi et al., 2009; Wei et al., 2016).

In addition to producing inflammatory cytokines, adipose tissue macrophages (ATMs) have also been postulated to perform beneficial functions during diet-induced obesity (DIO) (Fitzgibbons and Czech, 2016). They internalize excess free fatty acids (FFAs) released by insulin-resistant adipocytes, thereby buffering metabolic tissues from the damage caused by ectopic accumulation of saturated FFAs. They also clear dead adipocytes that accumulate during prolonged obesity when adipose tissue expands enough to produce hypoxia (Strissel et al., 2007; Sun et al., 2011). The clearance of these dead adipocytes promotes adipocyte turnover and maintains adipose tissue health during nutrient excess.

The diverse functions of macrophages, such as those described earlier, have often been conceptualized through an M1 and M2 paradigm (Gordon and Taylor, 2005). The M1 phenotype is caused by Th1 mediators such as lipopolysaccharide (LPS) and interferon gamma (IFNγ) and is characterized by increased production of pro-inflammatory cytokines, while the M2 phenotype is driven by Th2 mediators (e.g., interleukin-4 [IL-4]), which activates expression of immunosuppressive factors that promote macrophage clearance of dead cells and tissue remodeling (Odegaard et al., 2007). Although this M1/M2 paradigm has been a useful construct for understanding macrophage heterogeneity, studies suggest that it cannot adequately describe the functions of ATMs during obesity.

Studies from Xu et al., (2013) showed that macrophages from obese mice induce lysosomal and lipid metabolism pathways, raising the possibility that these pathways might help macrophages to clear dead adipocytes and their large FFA reservoirs. Moreover, studies from our laboratory showed that saturated FFAs produce a pro-inflammatory, metabolically activated (MMe) macrophage phenotype that is mechanistically distinct from M1 or M2 activation (Kratz et al., 2014). Although we showed that MMe macrophages accumulate in visceral and subcutaneous adipose tissue of obese humans and mice, their roles

in regulating macrophage inflammation, function, and insulin sensitivity have not been explored.

Here we combine proteomic and functional analyses with genetic models and dietary interventions to investigate the roles of MMe macrophages in DIO. We show that metabolic activation of macrophages induces inflammatory cytokine production (a detrimental function) and lysosomal exocytosis to dead adipocytes (a beneficial function). We identify NADPH oxidase 2 (NOX2) as a key regulator of the inflammatory cytokine expression and lysosomal exocytosis in MMe macrophages and show that ablating *Nox2* both improves and worsens the metabolic phenotype during DIO, depending on the duration of high-fat feeding. Collectively, our findings underscore the dynamic functions of ATMs during DIO and demonstrate the importance of the MMe phenotype in regulating these functions and their metabolic consequences.

RESULTS

Metabolic Activation Induces Macrophage Inflammation and Lysosomal Exocytosis In Vitro and In Vivo

We previously showed that saturated FFAs produce macrophage inflammation via an MMe pathway that is mechanistically distinct from the classically activated M1 phenotype induced by bacterial challenge (Kratz et al., 2014). Although we showed that these MMe macrophages are present in adipose tissue of obese humans and mice, their functions in DIO and insulin resistance are poorly understood.

To interrogate how metabolic activation might alter macrophage function, we produced pro-inflammatory MMe macrophages by treating murine bone marrow-derived macrophages (BMDMs) with glucose, insulin, and palmitate (Figure 1A) and performed plasma membrane proteomics. We focused on plasma membrane proteins because they mediate a variety of important macrophage functions, including phagocytosis, cell migration, and antigen presentation.

Mass spectrometric analysis of the plasma membrane identified 664 proteins in M0 (unstimulated) and MMe macrophages. Statistical analysis with the t test and G test identified 176 proteins that were differentially abundant (false discovery rate [FDR] < 0.05) in MMe versus M0 macrophages (Figure 1B). Gene ontology analysis of proteins induced in MMe macrophages identified enrichments in several annotations expected for a cell surface proteome (i.e., plasma membrane, membrane raft, and extracellular matrix) (Figure 1C), suggesting that our methods for isolating plasma membrane proteins were robust. Moreover, we observed increased levels of MMe-associated proteins (PLIN2 and P62), but not M1-associated proteins (CD40 and STAT1), that we previously identified in proteomic analyses of human MMe and M1 macrophages (Figure S1) (Kratz et al., 2014).

Unexpectedly, plasma membrane proteins induced in MMe macrophages were enriched in lysosomal membrane proteins ($p = 10^{-6}$) (Figure 1C; Table S1), and this enrichment was specific to the MMe phenotype, because they were not observed in M1 macrophages (Figure 1C). To confirm these observations using an alternative approach, we quantified cell surface LAMP1 and LAMP2 levels on M0, MMe, and M1 macrophages by flow cytometry. Consistent with our proteomics data, we found that LAMP1 and LAMP2 were induced on the cell surface of MMe, but not M1, macrophages (Figure 1D; Figure S1). Because lysosomal membrane proteins appear on the cell surface during lysosomal exocytosis, when lysosomal and plasma membranes fuse (Rodríguez et al., 1997), these findings suggest that metabolic activation induces macrophages to exocytose their lysosomes.

Previous studies showed that lysosomal exocytosis by macrophages is required for them to clear dead adipocytes (Haka et al., 2016). Because macrophages (~20 μm diameter) are much smaller than adipocytes (~120 μm diameter), they cannot clear dead adipocytes through a traditional phagocytosis mechanism. Instead, the macrophages form a tight attachment (a lysosomal synapse) on the dead adipocyte. They acidify the contact region using the plasma membrane proton pumping V-ATPase and secrete lysosomal contents into the lysosomal synapse. The lysosomal lipases in the acidic milieu liberate FFAs that are subsequently internalized by macrophages, leading to foam cell formation.

Because FFAs are required for metabolic activation, and dead adipocytes are an abundant reservoir of FFA, we hypothesized that dead adipocytes could induce the inflammation and lysosomal exocytosis associated with the MMe phenotype. To test this hypothesis, we treated unstimulated BMDMs with media conditioned by live or apoptotic 3T3-L1 adipocytes and measured inflammatory cytokine expression by qRT-PCR and quantified lysosomal exocytosis by staining for cell surface LAMP1 and LAMP2.

We found that media from apoptotic adipocytes coordinately induced the expression of *Il1β* and *Il6* (Figure 1E) and the appearance of cell surface LAMP1 and LAMP2 on macrophages (Figure 1F). The effects on cytokines and lysosomal exocytosis were specific to apoptotic adipocytes, because media from live 3T3-L1 adipocytes or apoptotic neutrophils (a dead cell without FFA) were incapable of inducing these changes (Figures 1E and 1F). Thus, dead adipocytes release factors that induce the inflammation and lysosomal exocytosis characteristic of MMe macrophages.

Our previous studies showed that ATMs from obese mice adopt an MMe phenotype (Kratz et al., 2014). We therefore reasoned that ATMs from obese mice would also show coordinated induction of cytokine expression and lysosomal exocytosis. To test this, we fed C57BL/6 mice a low-fat diet (LFD) or 45% high-fat diet (HFD) for 16 weeks, isolated ATMs (Figure 1G), confirmed their purity based on CD11c and F4/80 staining (98.1%) (Figure 1H), and assessed cytokine expression by qRT-PCR and cell surface lysosomal membrane protein levels by mass spectrometry.

Consistent with previous findings, ATMs from obese mice were characterized by elevated *Tnfα*, *Il6*, and *Il1β* expression (Figure 1I). Moreover, plasma membrane proteins elevated in ATMs from obese mice (relative to lean mice) were significantly enriched for lysosomal membrane proteins ($p = 10^{-7}$). Indeed, 10 lysosomal membrane proteins were induced on the cell surface of ATMs from obese mice (Figures 1J and 1K; Table S1), 6 of which (LAMP2, ATP6V1B2, ATP6V1A, AHNAK, NPC1, and ANXA2) were also induced on the cell surface of MMe macrophages in vitro.

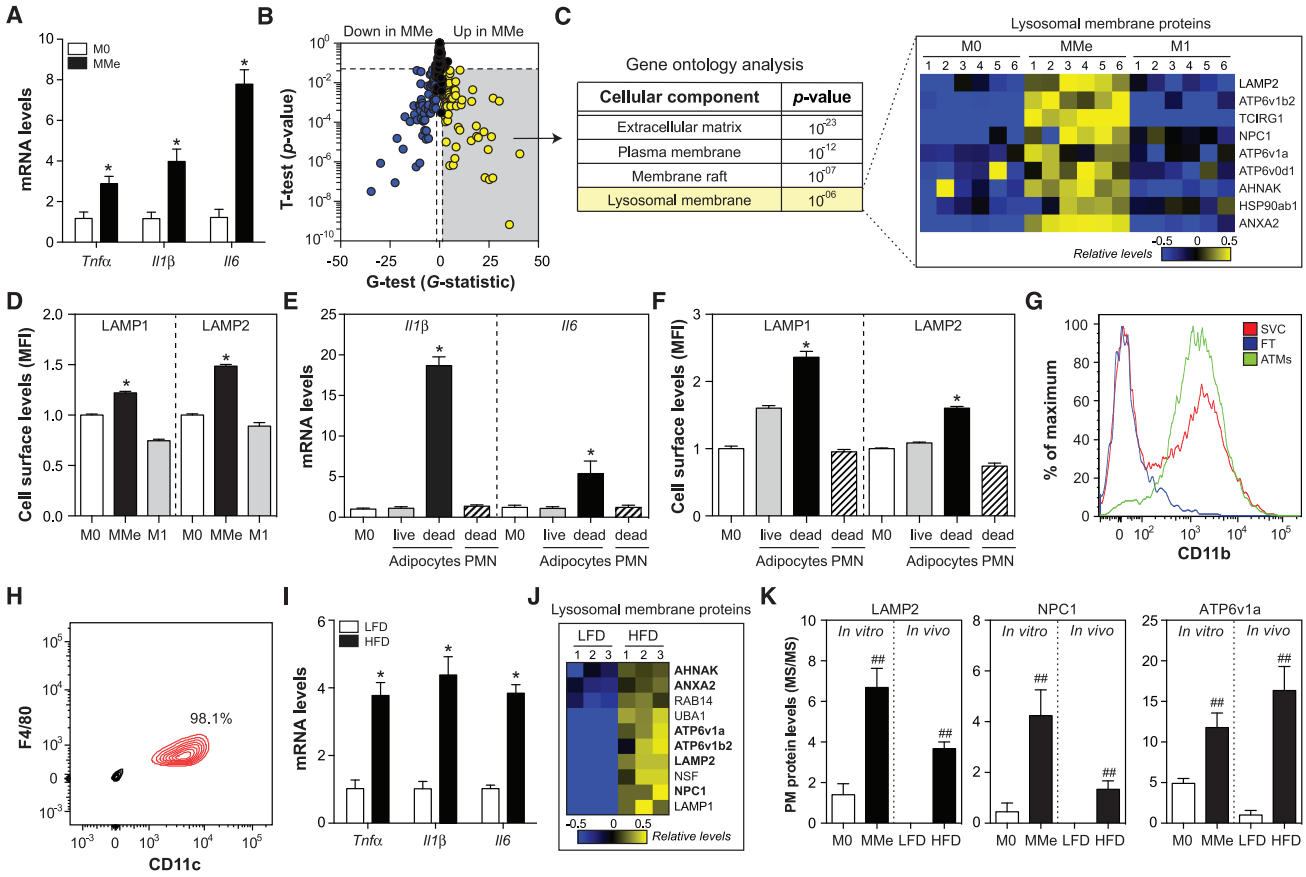

Figure 1. MMe Macrophages Overexpress Cytokines and Accumulate Cell Surface Lysosomal Membrane Proteins In Vitro and In Vivo

(A–D) BMDMs (M0) were metabolically activated (MMe) or classically activated (M1). (A) Inflammatory cytokine expression levels. (B) Plasma membrane proteomics analysis with the t test and G test identifies proteins induced (yellow) and suppressed (blue) on the cell surface of MMe macrophages (relative to M0). (C) Gene ontology analysis of plasma membrane proteins elevated on the cell surface of MMe macrophages (relative to M0). Relative abundances of proteins are presented as a heatmap. (D) Flow cytometric quantification of cell surface LAMP1 and LAMP2.

(E and F) BMDMs (M0) were treated with conditioned media collected from 3T3-L1 adipocytes (live or apoptotic) or apoptotic neutrophils (polymorphonuclear neutrophils [PMN]). (E) Inflammatory cytokine expression levels. (F) Flow cytometric quantification of cell surface LAMP1 and LAMP2.

(G–J) Analysis of ATMs from C57BL/6 mice fed a low-fat (LFD) or high-fat diet (HFD) for 16 weeks. (G) ATMs were isolated from the stromal vascular fraction (SVC) using anti-CD11b-coupled magnetic beads. ATM purity and recover were confirmed by staining for CD11b in the purified ATMs, SVC, and flowthrough (FT). (H) ATM purity was assessed by staining for CD11c and F4/80. (I) Inflammatory cytokine expression levels. (J) Heatmap of the relative abundance of cell surface lysosomal membrane proteins.

(K) A comparison of cell surface levels of LAMP2, NPC1, and ATP6v1a in vitro and in vivo; proteins were quantified by mass spectrometry.

Results are mean ± SEM; n = 3–6, *p < 0.05 Student's t test, ##p < 0.05 Student's t test and G > 1.5 G test. See also Figure S1 and Table S1.

TLR2, NOX2, and MYD88 Coordinately Regulate Inflammation and Lysosomal Exocytosis in MMe Macrophages

What signaling pathways regulate cytokine expression and lysosomal exocytosis in MMe macrophages? To begin to answer this question, we searched the literature for proteins known to mediate macrophage responses to FFAs, the driver of the MMe phenotype. We focused on toll-like receptor (TLR) 2, NOX2, MYD88, and TLR4 because previous studies showed that these proteins are required for palmitate-induced inflammation and/or endoplasmic reticulum (ER) stress in macrophages (Kratz et al., 2014; Robblee et al., 2016; Seimon et al., 2010).

We first investigated the effects of these knockouts on inflammatory cytokine expression. We found that ablating *Nox2* (*Gp91* subunit), *Tlr2*, *Myd88*, or *Tlr4* attenuated *Il6* and *Il1β* levels in MMe macrophages (Figure 2A; Figure S2). The anti-inflammatory effect of ablating *Nox2* or *Tlr2* was specific to MMe macrophages, because cytokine expression in M1 macrophages was unaffected (Figure 2A). In contrast, ablating *Tlr4* or *Myd88*, an adaptor protein used by most TLRs to activate nuclear factor κB (NF-κB) (Akira et al., 2001), lowered inflammatory cytokine expression in both MMe and M1 macrophages (Figure 2A; Figure S2). Altogether, these studies identified TLR2, NOX2, MYD88, and TLR4 as regulators of inflammatory cytokine expression in MMe macrophages and further demonstrated that distinct signaling pathways regulate inflammatory cytokine expression in MMe and M1 macrophages.

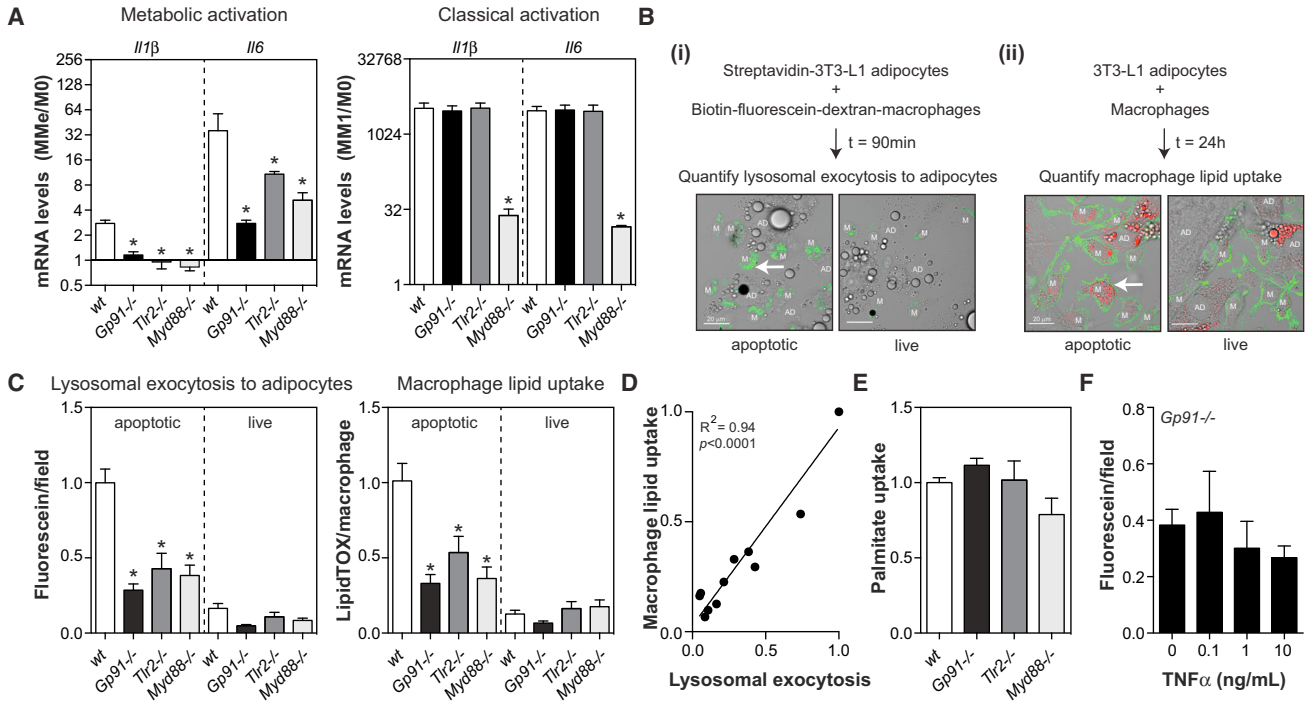

Figure 2. TLR2, NOX2, and MYD88 Coordinately Regulate Inflammatory Cytokine Expression and Lysosomal Exocytosis in MMe Macrophages

(A) Inflammatory cytokine expression in metabolically activated (MMe) macrophages and classically activated (M1) BMDMs made from wild-type (WT), TLR2-deficient (*Tlr2*$^{-/-}$), NOX2-deficient (*Gp91*$^{-/-}$), or MYD88-deficient (*Myd88*$^{-/-}$) mice. Levels are expressed relative to M0 for each genotype.

(B–D) Quantification of macrophage lysosomal exocytosis and lipid uptake from live or apoptotic 3T3-L1 adipocytes. (B) Schematic of the assay: (i) macrophage lysosomal exocytosis was quantified as the capture of previously endocytosed biotin-fluorescein-dextran (green) on the cell surface of streptavidin-labeled apoptotic adipocytes, and (ii) macrophage lipid uptake was quantified as the amount of LipidTOX signal (red) inside Alexa 444-CtB-labeled macrophages (green). Scale bar, 20 μm. (C) Quantification of lysosomal exocytosis and lipid uptake by WT, *Tlr2*$^{-/-}$, *Gp91*$^{-/-}$, or *Myd88*$^{-/-}$ BMDMs. (D) Relationship between macrophage lipid uptake and lysosomal exocytosis.

(E) Relative uptake of palmitate from the media by WT, *Tlr2*$^{-/-}$, *Gp91*$^{-/-}$, or *Myd88*$^{-/-}$ BMDMs.

(F) Lysosomal exocytosis by *Nox2*$^{-/-}$ macrophages pre-treated with TNF-α.

Results are mean ± SEM; n = 3–12, *p < 0.05 Student's t test. See also Figure S2.

We further investigated the effects of these knockouts on lysosomal exocytosis. To this end, we used a more physiologically relevant co-culture assay (Haka et al., 2016) that quantifies (1) the delivery of lysosomal contents from macrophages to apoptotic 3T3-L1 adipocytes and (2) the subsequent accumulation of adipocyte-derived lipids in the macrophage (Figure 2B). As a control, macrophages were co-incubated with live adipocytes, demonstrating the specificity of these processes to apoptotic adipocytes (Figure 2B).

We found that lysosomal exocytosis to apoptotic adipocytes was significantly impaired in *Nox2*$^{-/-}$, *Tlr2*$^{-/-}$, and *Myd88*$^{-/-}$ macrophages (Figure 2C). Moreover, *Nox2*$^{-/-}$, *Tlr2*$^{-/-}$, and *Myd88*$^{-/-}$ macrophages accumulated fewer lipids from apoptotic adipocytes (Figure 2C), perhaps due to their inability to deliver lysosomal lipases to mobilize FFAs from the adipocyte lipid droplet. Consistent with this interpretation, the extent of macrophage lipid accumulation was strongly and positively correlated ($R^2 = 0.94$, $p < 0.0001$) to the amount of lysosomal exocytosis (Figure 2D). Moreover, *Nox2*$^{-/-}$, *Tlr2*$^{-/-}$, and *Myd88*$^{-/-}$ macrophages were not defective in their ability to internalize palmitate (Figure 2E), one of the major FFAs liberated during lipolysis from adipocytes.

Lysosomal exocytosis to apoptotic adipocytes was not impaired in *Tlr4*$^{-/-}$ macrophages (Figure S2), even though this knockout suppressed inflammatory cytokine expression. These findings suggest that the defective lysosomal exocytosis observed in *Tlr2*$^{-/-}$, *Nox2*$^{-/-}$, and *Myd88*$^{-/-}$ macrophages was not reliant upon the suppression of inflammatory cytokines. Consistent with this hypothesis, supplementing *Nox2*$^{-/-}$ macrophages with tumor necrosis factor alpha (TNF-α), a key cytokine produced by ATMs, could not rescue the defect in lysosomal exocytosis (Figure 2F).

ATM Inflammation Precedes Visceral Fat Adipocyte Death during DIO

Our in vitro findings suggest that MMe macrophages might play complex roles during DIO. However, MMe macrophages overexpress inflammatory cytokines, which could promote insulin resistance (Chawla et al., 2011; Olefsky and Glass, 2010). However, MMe macrophages exocytose their lysosomes and clear

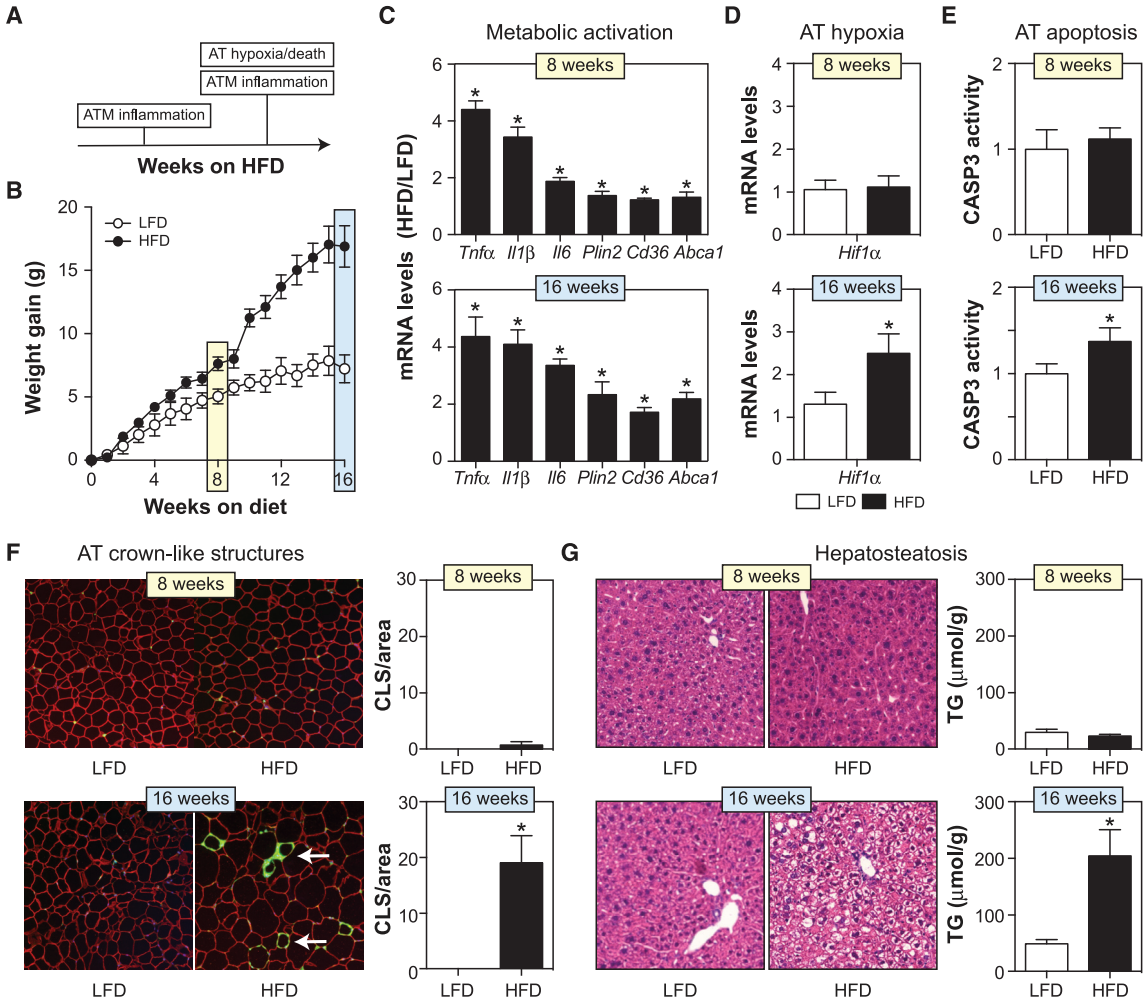

Figure 3. ATM Inflammation Precedes Visceral Fat Adipocyte Death during DIO

Wild-type C57BL/6 mice were fed a low-fat diet (LFD) or 45% high-fat diet (HFD) for 8 or 16 weeks.

(A) A model for the timing of ATM inflammation and epididymal fat death during DIO.

(B) Body weight gain.

(C) mRNA expression of inflammatory cytokines and lipid metabolism genes in purified ATMs.

(D) *Hif1α* mRNA levels in epididymal fat (a marker of hypoxia).

(E) Caspase-3 (CASP3) activity levels in epididymal fat.

(F) Epididymal fat was stained with antibodies against PLIN2 (red, identifies adipocytes), MAC2 (green, identifies macrophages), and DAPI (blue, identifies nuclei). Macrophages in crown-like structures (CLSs, arrow) were quantified by microscopy and standardized per unit area.

(G) H&E staining of liver and quantification of liver triglyceride (TG) levels.

Results are mean ± SEM; n = 5–15, *p < 0.05 Student's t test. See also Figures S3 and S4.

dead adipocytes, which could limit insulin resistance by maintaining adipose tissue health and protecting against ectopic lipid deposition in the liver (Shulman, 2014; Strissel et al., 2007; Sun et al., 2011). Because these potentially detrimental and beneficial properties of MMe macrophages are coordinately regulated by TLR2, NOX2, and MYD88, we reasoned that interpreting the metabolic phenotypes of mice deficient in one or more of these proteins might be challenging.

To help facilitate interpretation, we first determined whether ATM inflammation and adipocyte death (and hence the need for dead adipocyte clearance) occurred at different time points during DIO. Previous studies showed that ATM inflammation might be an early and persistent event, while adipocyte death may predominantly occur after prolonged high-fat feeding when adipose tissue becomes hypoxic (Figure 3A) (Strissel et al., 2007). However, these studies were performed in mice fed a 60% HFD, and our studies used the 45% HFD. To better understand the timing of these events and to establish reproducible conditions to investigate the effects of our knockouts on these processes in vivo, we studied adipose tissue biology in wild-type C57BL/6 mice fed an LFD or 45% for 8 and 16 weeks (Figure 3B).

Eight weeks of high-fat feeding was sufficient to induce the MMe phenotype in ATMs characterized by increased inflammatory cytokines (*Tnfα*, *Il6*, and *Il1β*) and genes involved in lipid metabolism (*Plin2*, *Abca1*, and *Cd36*) (Figure 3C). Despite the presence of ATM inflammation, several lines of evidence indicated that epididymal fat health in obese mice was not significantly compromised at this time point. First, adipose tissue levels of *Hif1α* were not elevated (Figure 3D), suggesting that hypoxia, a key driver of adipocyte death (Wang et al., 1995), had not yet occurred. Second, adipose tissue caspase-3 activity, a marker of apoptosis (Nicholson et al., 1995), was not elevated (Figure 3E). Third, the number of crown-like structures, an indicator of adipocyte death (Murano et al., 2008), was unchanged (Figure 3F; Figure S3). Finally, ectopic fat deposition in the liver, which has been associated with adipocyte death in visceral fat (Strissel et al., 2007), was undetectable (Figure 3G; Figure S4).

Although ATMs still overexpressed the cytokines and lipid metabolism genes characteristic of MMe macrophages following 16 weeks of high-fat feeding (Figure 3C), the state of epididymal fat health was substantially different at this time point. Adipose tissue *Hif1α* levels were elevated (Figure 3D), suggesting that the tissue was hypoxic. Moreover, adipose tissue caspase-3 activity and crown-like structures were markedly increased (Figures 3E and 3F; Figure S3), indicating the presence of apoptotic adipocytes. Consistent with the deterioration of epididymal fat health and increased FFA release, the MMe phenotype was more pronounced at this time point, particularly with respect to the lipid metabolism genes (Figure 3C). Moreover, ectopic fat deposition in the liver was detectable in obese mice (Figure 3G; Figure S4), and this deposition could not be explained by changes in genes involved in triglyceride (TG) synthesis (*Fas1*, *Acc1*, and *Srebp1*) or fatty acid metabolism (*Pparα* and *Cpt1α*) in the liver (Figure S4).

These findings suggest that while MMe ATMs are present at both 8 and 16 weeks of 45% high-fat feeding, adipocyte death, and hence the requirement for macrophages to clear dead adipocytes, may only be an important consideration after 16 weeks of high-fat feeding.

Nox2$^{-/-}$ Mice Have Improved ATM Inflammation and Glucose Tolerance after 8 Weeks of High-Fat Feeding

Our identification of NOX2, TLR2, and MYD88 as drivers of cytokine expression and lysosomal exocytosis in MMe macrophages provided an opportunity to inhibit these processes in vivo and assess effects on obesity-associated insulin resistance. We focused our initial studies on *Nox2*$^{-/-}$ mice because NOX2 is predominantly expressed by phagocytic cells, including macrophages and neutrophils (Bedard and Krause, 2007).

We began by interrogating the metabolic phenotypes of *Nox2*$^{-/-}$ mice following 8 weeks of high-fat feeding. Because ATM inflammation was present at this time point, but adipocyte apoptosis had not yet occurred (Figure 3), we hypothesized that the anti-inflammatory effect of *Nox2*$^{-/-}$ would predominate and protection from metabolic derailments during DIO would be observed at this early time point. This hypothesis makes several predictions.

First, ablating *Nox2* should attenuate ATM inflammation. Although *Nox2*$^{-/-}$ mice fed the HFD were heavier than wild-type mice (Figure 4A), ATMs isolated from visceral fat were substantially less inflamed, as evidenced by decreased expression of *Tnfα*, *Il6*, and *Il1β* (Figure 4B). Because NOX2 drives inflammatory cytokine expression in MMe, but not M1, macrophages (Figure 2), these findings reinforce the notion that ATMs are inflamed via an MMe pathway in vivo (Kratz et al., 2014).

Second, ablating *Nox2* should not increase the number of dead adipocytes. *Nox2*$^{-/-}$ mice showed no differences in adipocyte death indicators; *Hif1α* levels, caspase-3 activity, and the number crown-like structures were unchanged, and ectopic fat accumulation in the liver was only minimally and insignificantly increased in *Nox2*$^{-/-}$ mice relative to wild-type mice fed the HFD (Figures 4C–4F; Figures S3 and S4). Moreover, none of these adipocyte death indicators were elevated in obese relative to lean mice, irrespective of genotype (Figures 4C–4F), which is consistent with our findings that 8 weeks of 45% HFD is insufficient to induce adipocyte death (Figure 3).

Third, this hypothesis predicts that *Nox2*$^{-/-}$ mice should demonstrate improved metabolic parameters. *Nox2*$^{-/-}$ mice fed the HFD had lower fasting glucose levels (Figure 4G) and improved glucose tolerance (Figure 4H). However, fasting insulin levels and insulin tolerance remained unchanged (Figures 4G and 4I), perhaps due to the increased body weight, the mild hepatosteatosis, and the increased number of ATMs in *Nox2*$^{-/-}$ mice (Figure S5), all of which would limit the anti-inflammatory effect of the knockout.

Altogether, these findings provide further evidence that ATMs are inflamed via an MMe pathway in vivo and further suggest that inhibiting inflammatory cytokine expression in MMe macrophages (by ablating *Nox2*) protects against metabolic dysfunction following 8 weeks of high-fat feeding.

Nox2$^{-/-}$ Mice Develop Severe Visceral Lipoatrophy, Hepatosteatosis, and Insulin Resistance following 16 Weeks of HFD

Next, we investigated the metabolic phenotypes of *Nox2*$^{-/-}$ mice fed a HFD for 16 weeks. Because ATM inflammation and adipocyte death were both present at this time point (Figure 3), and ablating *Nox2* attenuated metabolic activation and lysosome secretion in response to dead adipocytes (Figure 2), we hypothesized that *Nox2*$^{-/-}$ mice might exhibit a more complex phenotype at this later time point. To explore this, we characterized the adipose tissue, liver, and metabolic parameters of *Nox2*$^{-/-}$ mice fed the HFD for 16 weeks.

The protection observed in *Nox2*$^{-/-}$ mice following 8 weeks of HFD was reversed after prolonged high-fat feeding. *Nox2*$^{-/-}$ mice fed a HFD for 16 weeks were more obese, hyperglycemic, hyperinsulinemic, and insulin resistant than wild-type controls (Figures 5A–5D). *Nox2*$^{-/-}$ mice retained glucose tolerance, but they required higher levels of insulin production to maintain glucose homeostasis (Figure 5C).

An examination of the epididymal fat in *Nox2*$^{-/-}$ mice fed the HFD for 16 weeks revealed marked increases in the number of crown-like structures (Figure 5E; Figure S3) and caspase-3 activity (Figure 5F) relative to control mice, suggesting a higher accumulation of dead adipocytes. The extent of this adipocyte death was substantial given that *Nox2*$^{-/-}$ mice fed the HFD had less epididymal fat mass than wild-type mice (Figure 5G), despite

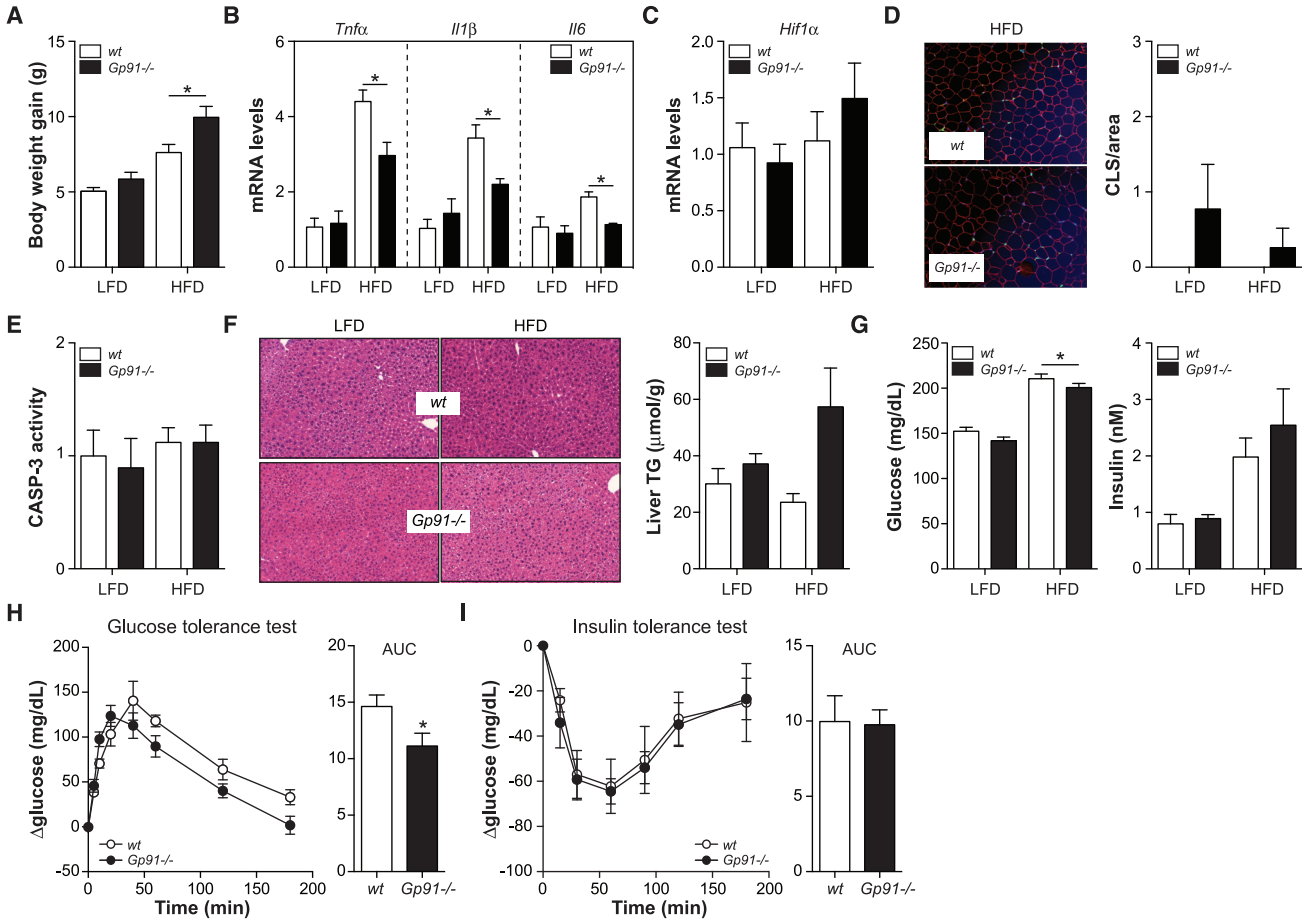

Figure 4. *Nox2*$^{-/-}$ Mice Have Improved ATM Inflammation and Glucose Tolerance after 8 Weeks of HFD

Wild-type (WT) and *Gp91*$^{-/-}$ mice were fed a low-fat diet (LFD) or 45% high-fat diet (HFD) for 8 weeks.

(A) Body weight gain.

(B) Inflammatory cytokine expression in purified ATMs.

(C) *Hif1*α mRNA levels in epididymal fat (a marker of hypoxia).

(D) Epididymal fat was stained with antibodies against PLIN2 (red, identifies adipocytes), MAC2 (green, identifies macrophages), and DAPI (blue, identifies nuclei). Macrophages in crown-like structures (CLSs, arrow) were quantified by microscopy and standardized per unit area.

(E) Caspase-3 (CASP3) activity levels in epididymal fat.

(F) H&E staining of liver and quantification of liver triglyceride (TG) levels.

(G) Fasting blood glucose levels and serum insulin levels.

(H and I) Glucose tolerance (H) and insulin tolerance (I) tests in WT and *Gp91*$^{-/-}$ mice fed the HFD. Glucose tolerance and insulin tolerance were assessed by area under the curve (AUC) analysis.

Results are mean ± SEM; n = 5–15, *p < 0.05 Student's t test. See also Figures S3–S5.

being more obese (Figure 5A). In contrast, *Nox2*$^{-/-}$ mice had more epididymal fat than wild-type mice following 8 weeks of HFD (Figure 5G). These findings suggest that *Nox2*$^{-/-}$ mice are capable of expanding their epididymal fat mass during early DIO but that they cannot sustain it during prolonged exposure to the HFD.

Despite the increased number of dead adipocytes in *Nox2*$^{-/-}$ mice, which should induce macrophage inflammation (Figure 1), ATM expression of *Tnf*α, *Il6*, and *Il1*β was similar to that of wild-type mice (Figure 5H). Thus, it is likely that the anti-inflammatory effect of ablating *Nox2* was still present at 16 weeks but masked by the hyper-inflammatory environment produced by the dead adipocytes.

Consistent with the deterioration of epididymal fat health and mass at 16 weeks of HFD, *Nox2*$^{-/-}$ mice displayed severe hepatosteatosis, characterized by increased hepatic TG mass and liver weight (Figures 5I–5K; Figure S4), This hepatosteatosis could not be explained by changes in the expression of liver genes involved in TG synthesis (*Fas1*, *Acc1*, and *Srebp1*) or fatty acid metabolism (*Ppar*α and *Cpt1*α) (Figure 5L).

Altogether, these studies showed that *Nox2*$^{-/-}$ mice develop severe late-onset adipocyte death, hepatosteatosis, and insulin resistance. Because *Nox2*$^{-/-}$ mice are more obese than their wild-type counterparts, we explored the possibility that these late-onset effects were due to excess body mass. To test this, we fed wild-type mice a HFD until their average body weight

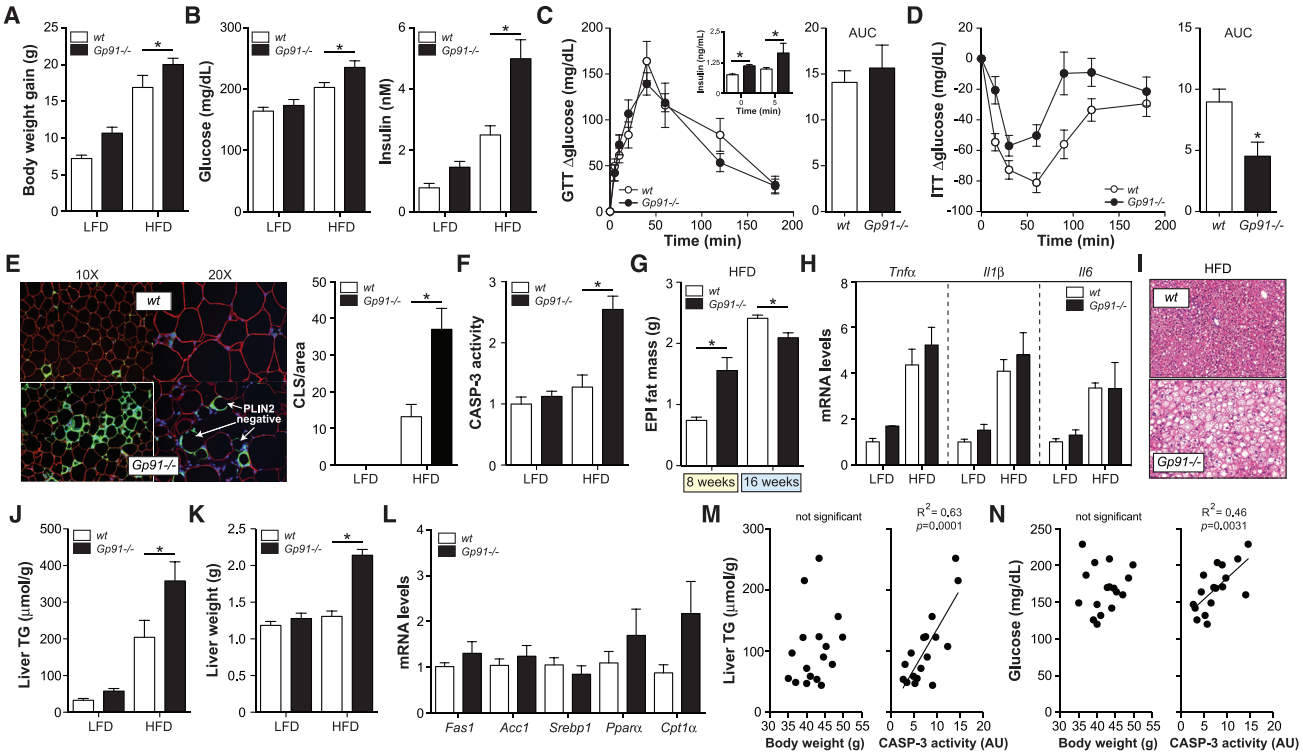

Figure 5. *Nox2*$^{-/-}$ Mice Develop Severe Visceral Lipoatrophy, Hepatosteatosis, and Insulin Resistance following 16 Weeks of HFD

Wild-type (WT) and *Gp91*$^{-/-}$ mice were fed a low-fat diet (LFD) or 45% high-fat diet (HFD) for 16 weeks.

(A) Body weight gain.

(B) Fasting blood glucose levels and serum insulin levels.

(C and D) Glucose tolerance test (GTT) (C) and insulin tolerance test (ITT) (D) in WT and *Gp91*$^{-/-}$ mice fed the HFD. Insulin levels during the GTT are shown in the inset. Glucose tolerance and insulin tolerance were assessed by area under the curve (AUC) analysis.

(E) Epididymal fat was stained with antibodies against PLIN2 (red, identifies adipocytes), MAC2 (green, identifies macrophages), and DAPI (blue, identifies nuclei). Macrophages in crown-like structures (CLSs, arrow) were quantified by microscopy and standardized per unit area.

(F) Caspase-3 (CASP3) activity levels in epididymal fat.

(G) Epididymal fat mass following in WT and *Gp91*$^{-/-}$ mice following 8 and 16 weeks of HFD.

(H) Inflammatory cytokine expression in purified ATMs.

(I) H&E staining of liver.

(J) Liver triglyceride (TG) levels.

(K) Liver weight.

(L) Hepatic expression of genes involved in TG synthesis and metabolism in mice fed the HFD.

(M and N) Linear regression analysis of body weight or epididymal fat caspase-3 activity versus liver TGs (M) and fasting glucose levels (N).

Results are mean ± SEM; n = 5–15, *p < 0.05 Student's t test. See also Figures S3–S6.

matched *Nox2*$^{-/-}$ mice at 16 weeks (wild-type match) and quantified key aspects of the metabolic phenotype.

We found that wild-type-match mice could not mimic the late-onset dead adipocyte accumulation, hepatosteatosis, and insulin resistance observed in *Nox2*$^{-/-}$ mice (Figures S3, S4, and S6), suggesting that these metabolic abnormalities were not driven by the increased body weight of *Nox2*$^{-/-}$ mice fed the HFD. Liver TGs and fasting glucose levels were not correlated to body weight in wild-type and *Nox2*$^{-/-}$ mice fed the HFD (Figures 5M and 5N). In contrast, these parameters were significantly and positively correlated to the extent of adipocyte death in epididymal fat, as determined by caspase-3 activity (Figures 5M and 5N). Thus, the inability of *Nox2*$^{-/-}$ mice to sustain their epididymal fat may help to explain the late-onset hepatosteatosis and metabolic defects observed in these mice.

Dead Adipocyte Accumulation Is Associated with Defective Lysosomal Exocytosis by *Nox2*$^{-/-}$ ATMs

In principle, the number of dead adipocytes observed in vivo is determined both by the rate of death and the rate of clearance (Figure 6A); the latter process, which is mediated by ATMs, has not been the subject of intensive study. Because *Nox2*$^{-/-}$ macrophages exhibited defective lysosomal exocytosis and clearance of apoptotic adipocytes in vitro (Figures 1 and 2), we reasoned that defective dead adipocyte clearance by ATMs might help to explain the late-onset accumulation of dead adipocytes. We used three approaches to test this hypothesis.

First, we investigated whether drivers of adipocyte death were elevated in *Nox2*$^{-/-}$ mice. Adipocyte apoptosis can be caused by hypoxia and/or inflammation (Sun et al., 2011), both of which increase as adipose tissue expands during obesity. Neither of

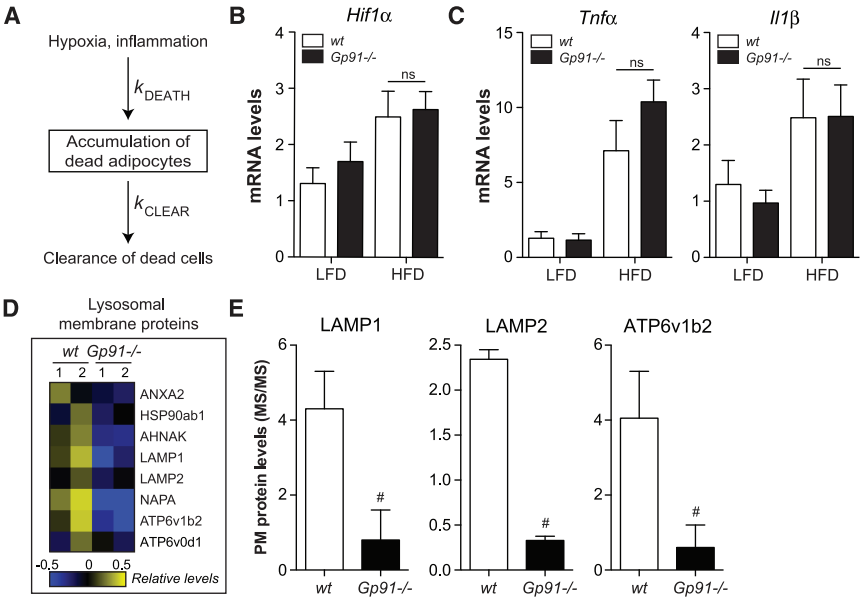

Figure 6. ATMs from Obese *Nox2*$^{-/-}$ Mice Exhibit Lower Levels of Lysosomal Membrane Proteins on the Cell Surface

Wild-type (WT) and *Gp91*$^{-/-}$ mice were fed a low-fat diet (LFD) or 45% high-fat diet (HFD) for 16 weeks.

(A) A model for the determinants of dead adipocyte number in vivo.

(B) *Hif1α* mRNA levels in epididymal fat (a marker of hypoxia).

(C) Inflammatory cytokine expression levels in epididymal fat.

(D and E) ATMs were purified from WT and *Gp91*$^{-/-}$ mice and interrogated by plasma membrane proteomics. (D) Heatmap of the relative abundance of cell surface lysosomal membrane proteins. (E) Examples of several lysosomal membrane proteins on the cell surface of ATMs; proteins were quantified by mass spectrometry.

Results are mean ± SEM; n = 2–5, $^{\#}p < 0.05$ G test. See also Table S1.

these mechanisms are a likely cause of dead adipocyte accumulation in *Nox2*$^{-/-}$ mice, because adipose tissue levels of *Hif1α* (hypoxia marker) and *Tnfα* and *Il1β* (pro-inflammatory markers) were unchanged after 16 weeks of high-fat feeding compared to wild-type mice (Figures 6B and 6C). Moreover, ATM inflammation (Figure 5) and ATM number (Figure S5) were not significantly different between wild-type and *Nox2*$^{-/-}$ mice fed the HFD.

Second, we determined whether ATMs from *Nox2*$^{-/-}$ mice had lower cell surface levels of lysosomal membrane proteins, the hallmark of lysosomal exocytosis (Rodríguez et al., 1997). We isolated ATMs from HFD-fed wild-type and *Nox2*$^{-/-}$ mice and interrogated them by plasma membrane proteomics. This analysis identified 8 lysosomal membrane proteins on the cell surface of wild-type ATMs, all of which were lower on the cell surface of ATMs from *Nox2*$^{-/-}$ mice (Figures 6D and 6E; Table S1). The decreased levels of lysosomal membrane proteins on *Nox2*$^{-/-}$ ATMs were likely underestimated given that *Nox2*$^{-/-}$ mice had significantly more dead adipocytes, which should stimulate lysosomal exocytosis (Figures 1 and 2). These findings suggest that ATMs from *Nox2*$^{-/-}$ mice exhibit impaired lysosomal exocytosis in vivo.

Third, we determined whether ablating *Nox2* in myeloid cells specifically could reproduce the late-onset accumulation of dead adipocytes and associated metabolic derailments. We crossed *Nox2*$^{fl/fl}$ mice with *LysM-Cre*$^{+/-}$ mice to generate myeloid cell-specific, *Nox2*-deficient mice (*Nox2*$^{fl/fl}$*LysM-Cre*$^{+/-}$) and littermate controls (*Nox2*$^{fl/fl}$*LysM-Cre*$^{-/-}$). After validating *Nox2* knockout in ATMs (Figure S7), we examined the metabolic phenotypes of these mice following prolonged high-fat feeding.

Myeloid cell-specific ablation of *Nox2* mimicked the late-onset accumulation of dead adipocytes in the absence of increased hypoxia or adipose tissue inflammation (Figures 7A–7D; Figure S3), hepatosteatosis and increased liver weight (Figures 7E and 7F; Figure S4), obesity (Figure 7G), hyperglycemia (Figure 7H), and hyperinsulinemia (Figure 7I) phenotypes of the whole-animal knockout. The stronger increase in the number of crown-like structures in the LysM-Cre model relative to the global knockout was due to the presence of fewer crown-like structures in LysM-Cre$^{-/-}$ control mice, which likely reflects the variability in the appearance of crown-like structures in vivo.

These findings suggest that the accumulation of dead adipocytes and the associated metabolic dysfunction are driven by the loss of *Nox2* in myeloid cells, not an unanticipated effect in adipocytes.

DISCUSSION

Accumulating evidence suggests that ATMs perform both detrimental and beneficial functions during obesity. They produce inflammatory cytokines that promote insulin resistance (Chawla et al., 2011; Olefsky and Glass, 2010). They also might protect metabolic tissues from the deleterious effects of excess FFAs and contribute to adipose tissue homeostasis by clearing dead adipocytes. Traditionally, these diverse functions have been attributed to distinct ATM populations; the detrimental functions have been associated with M1-like macrophages, which may predominate during early DIO (Lumeng et al., 2007), while the beneficial functions have been ascribed to M2-like macrophages, which may accumulate during prolonged DIO (Shaul et al., 2010).

Here we provide evidence that inflammatory cytokine production and dead adipocyte clearance are functional properties of a single MMe macrophage phenotype that is present during early and late DIO. We further show that inflammatory signaling through NOX2, TLR2, and MYD88 coordinately regulates both the detrimental and the beneficial functions of MMe macrophages. Accordingly, ablating *Nox2* produces a complex metabolic phenotype determined by the duration of high-fat feeding, which in turn highlights the relative importance of macrophage

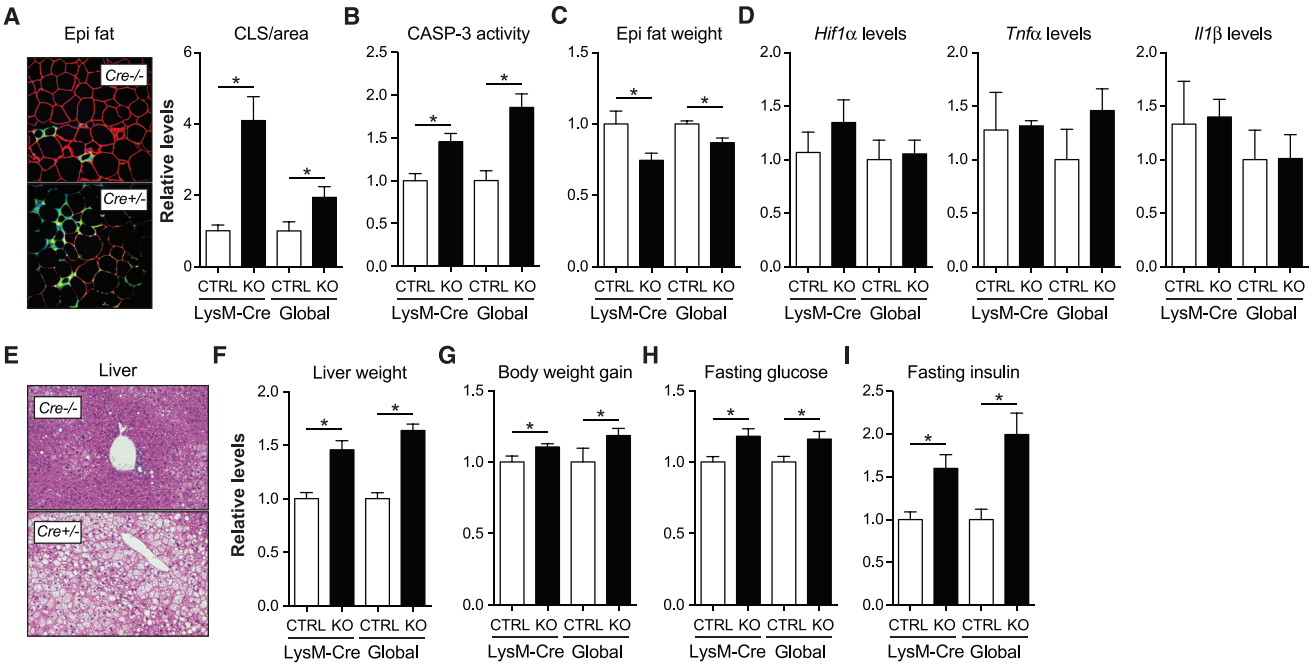

Figure 7. Ablating *Nox2* in Myeloid Cells Is Sufficient to Produce Late-Onset Lipoatrophy, Hepatosteatosis, and Insulin Resistance

A comparison of the late-onset phenotypes in whole-animal, NOX2-deficient (global knockout [KO]), and myeloid cell-deficient (LysM-Cre KO) mice fed the HFD. All parameters are plotted relative to the appropriate wild-type control (CTRL).

(A) Epididymal fat was stained with antibodies against PLIN2 (red, identifies adipocytes), MAC2 (green, identifies macrophages), and DAPI (blue, identifies nuclei). Macrophages in crown-like structures (CLSs, arrow) were quantified by microscopy and standardized per unit area.

(B) Relative caspase-3 (CASP3) activity in epididymal fat.

(C) Relative epididymal fat mass.

(D) Relative levels of *Hif1α* (a hypoxia marker) and *Tnfα* and *Il1β* (inflammatory markers) in epididymal fat.

(E) H&E staining of the liver.

(F) Relative liver weight.

(G) Relative body weight gain.

(H and I) Relative fasting glucose (H) and insulin (I) levels. Data for the global control and KO mice are re-presented in modified form for comparative purposes. Results are mean ± SEM; n = 5–10, *p < 0.05 Student's t test. See also Figures S3, S4, and S7.

inflammation and dead adipocyte clearance during the progression of obesity.

After 8 weeks of HFD, wild-type mice exhibited ATM inflammation in the absence of adipose tissue hypoxia and adipocyte death, indicating a low need for dead adipocyte clearance at this time point. Accordingly, the anti-inflammatory benefit of ablating *Nox2* was observed without exposing the costs associated with impaired dead adipocyte clearance. *Nox2*$^{-/-}$ mice had attenuated ATM inflammation and exhibited improvements in fasting glucose and glucose tolerance, even though mice were more obese, had more ATMs in epididymal fat, and were trending to hepatosteatosis—all of which should exacerbate metabolic dysfunction during DIO. Because ablating *Nox2* inhibits inflammation in MMe macrophages, but not M1 macrophages, our findings further underscore the importance of metabolic activation in producing ATM inflammation in obesity.

In contrast, after 16 weeks of HFD, we found that dead adipocytes accumulated in epididymal fat of wild-type mice, and this accumulation was significantly exacerbated in *Nox2*$^{-/-}$ mice, suggesting that the costs associated with impaired dead adipocyte clearance were evident at this time point.

Three lines of evidence suggest that this late-onset dead adipocyte accumulation in *Nox2*$^{-/-}$ mice was due to impaired clearance by ATMs. First, we showed that inflammation and hypoxia, the main drivers of adipocyte death, were not increased in *Nox2*$^{-/-}$ mice relative to wild-type mice. Second, we showed that ablating *Nox2* interfered with dead adipocyte clearance through lysosomal exocytosis in vitro and further showed that *Nox2*$^{-/-}$ ATMs had impaired lysosomal exocytosis in vivo. Third, we showed that mice lacking *Nox2* in myeloid cells specifically reproduced this late-onset phenotype. Although neutrophils are also targeted by the LysM-Cre system (Clausen et al., 1999), ATMs are the most abundant cell type in adipose tissue and form the adipocyte-clearing crown-like structures during DIO. It is therefore unlikely that neutrophils significantly contribute to the impaired adipocyte clearance observed in vivo. However, because neutrophils promote insulin resistance during DIO (Talukdar et al., 2012), we cannot ignore their potential contribution to the metabolic phenotypes observed in the *Nox2*$^{-/-}$ mice. Collectively, these findings implicate MMe ATMs and their ability to exocytose their lysosomes to dead adipocytes as a key determinant of adipose tissue remodeling and health during prolonged obesity.

The late-onset dead adipocyte accumulation was so extensive in *Nox2*$^{-/-}$ mice that they had less epididymal fat mass than their wild-type counterparts despite being more obese, suggesting that visceral fat could no longer store excess dietary nutrients. This phenotype shares some similarities with lipodystrophy, in which the inability to store nutrients in adipose tissue results in ectopic fat accumulation in the liver and hepatosteatosis, which in turn drives insulin resistance (Fiorenza et al., 2011). *Nox2*$^{-/-}$ mice fed the HFD for 16 weeks exhibited severe hepatosteatosis, which was likely responsible for the hyperglycemia, hyperinsulinemia, and insulin resistance at this time point (Cohen et al., 2011; Shulman, 2014).

However, unlike lipodystrophy, *Nox2*$^{-/-}$ mice did not exhibit inherent defects in adipose tissue development or expansion. Epididymal fat in *Nox2*$^{-/-}$ mice fed the LFD was normal at both time points. Furthermore, epididymal fat mass was higher in *Nox2*$^{-/-}$ mice fed the HFD for 8 weeks relative to wild-type mice. Instead, *Nox2*$^{-/-}$ mice had a diminished capacity to maintain their epididymal fat during prolonged nutrient excess, when adipose tissue hypoxia and adipocyte death were apparent, and ATM-mediated dead adipocyte clearance was required.

The clearance of dead adipocytes poses two unique challenges for macrophages. First, because adipocytes are so large, macrophages cannot phagocytose them. Instead, their clearance relies on the formation of extracellular lysosomal compartments between many macrophages and one adipocyte (Haka et al., 2016), resulting in the formation of crown-like structures. Second, adipocytes are predominantly composed of TGs. Thus, during clearance, macrophages are exposed to FFAs such as palmitate, which induce macrophage inflammation (Kratz et al., 2014). For this reason, clearance of dead adipocytes, unlike clearance of other dead cells (Fadok et al., 1998), is an inflammation-propagating event. Crown-like structures have been positively correlated with inflammation in adipose tissue of obese humans and mice (Lumeng et al., 2007).

From this perspective, the MMe macrophage is well positioned to handle the unique challenges imposed by dead adipocytes. FFAs released by dead adipocytes promote the MMe macrophage phenotype and its associated upregulation of lysosomal exocytosis, lipid metabolism, and inflammation. Lysosomal exocytosis may drive FFA liberation to help clear the TG droplet, which may be further enabled by the induction of lysosomal genes reported in ATMs from morbidly obese mice (Xu et al., 2013). Increased expression of lipid metabolism genes (i.e., ABCA1, CD36, and PLIN2) could help macrophages to productively handle this excess fat, while inflammation could facilitate recruitment of additional macrophages to the crown-like structure to assist in clearance.

Prolonged macrophage inflammation also carries its consequences. Cytokines such as TNF-α promote damage to metabolic organs and drive insulin resistance during obesity (Hotamisligil et al., 1993) and our findings during early DIO provide further support for this widely accepted paradigm.

However, studies showed that the metabolic consequences of this inflammation might not be as straightforward as this paradigm suggests. For example, thermoneutral housing accelerated the onset of adipose tissue inflammation but did not worsen the metabolic phenotype (Tian et al., 2016). Similarly, ablating TNF-α expression by adipocytes exacerbated obesity-associated insulin resistance and hepatosteatosis (Wernstedt Asterholm et al., 2014).

Our findings reinforce the emerging complex relationship among inflammation, macrophages, and metabolic phenotypes during DIO. We observed contradictory metabolic phenotypes with the same anti-inflammatory perturbation (*Nox2*$^{-/-}$) over two time points during DIO. Previous studies with *Nox2*$^{-/-}$ mice fed the HFD reported similar contradictory findings. One study reported improvements in fasting glucose, glucose tolerance, and brain injury in *Nox2*$^{-/-}$ mice fed a 60% HFD for 14 weeks (Pepping et al., 2013). Another study showed increased adiposity due to hyperphagia and worsened insulin resistance and hepatosteatosis in *Nox2*$^{-/-}$ fed a 60% HFD for 18 weeks (Costford et al., 2014).

Although we cannot rule out the contribution of other NOX2-driven mechanisms, the contradictory findings that we and others report with *Nox2*$^{-/-}$ mice may be conceptualized by integrating the beneficial and detrimental functions of ATMs through a single MMe phenotype, whose impact on adipose tissue biology and metabolic phenotypes is determined by the duration of high-fat feeding. Future experiments will be required to determine whether this paradigm holds true in other anti-inflammatory settings.

EXPERIMENTAL PROCEDURES

Mice

All animal studies were approved by the University of Chicago Institutional Animal Care and Use Committee (ACUP 72209). Wild-type, *Gp91*$^{-/-}$, *Tlr2*$^{-/-}$, *Tlr4*$^{-/-}$, and *Myd88*$^{-/-}$ male mice on the C57BL/6 background are from Jackson Laboratory. For DIO studies, wild-type, *Gp91*$^{-/-}$, *Tlr2*$^{-/-}$, and *Tlr4*$^{-/-}$ mice were placed on an LFD or HFD (45% fat, Research Diets, D12451) at 8 weeks of age for up to 16 weeks.

Nox2$^{fl/fl}$ Mice

Nox2$^{fl/fl}$ mice were described (Sag et al., 2017) and were crossed with *LysM-cre* knockin mice (Jackson Laboratory, 004781) to generate LysM-cre$^{+/-}$ *Nox2*$^{fl/fl}$ mice and littermate control *Nox2*$^{fl/fl}$ mice. See Supplemental Experimental Procedures for genotyping details.

Differentiation and Activation of BMDMs

Murine BMDMs were differentiated from bone marrow stem cells as previously described (Kratz et al., 2014). For M1 activation, BMDMs were treated with LPS (5 ng/mL) and IFNγ (12 ng/mL) for 24 hr. For MMe activation, macrophages were treated with a combination of glucose (30 mM), insulin (10 nM), and palmitate (0.4 mM) for 24 hr. Macrophages were also treated with media conditioned by live 3T3-L1 adipocytes, apoptotic 3T3-L1 adipocytes, or apoptotic neutrophils for 24 hr.

Macrophage Clearance of Apoptotic Adipocytes

Macrophage clearance of apoptotic adipocytes and subsequent accumulation of lipids were performed as previously described (Haka et al., 2016). See Supplemental Experimental Procedures for additional details.

ATM Isolation and Analysis

ATMs were isolated using anti-CD11b antibody coupled to magnetic beads as previously described (Kratz et al., 2014), and purity was assessed by flow cytometry. ATMs were interrogated by qRT-PCR, plasma membrane proteomics, and flow cytometry. A workflow for flow cytometric analysis of ATMs is provided in the Supplemental Information (Figure S5).

Plasma Membrane Proteomics

Plasma membrane proteins of BMDMs or ATMs were isolated and analyzed by mass spectrometry as previously described (Becker et al., 2012). Proteins were quantified by spectral counting and statistical significance was assessed using a combination of the G test (G statistic) and t test (p value) with correction for the false discovery rate as previously described (Heinecke et al., 2010).

Plasma Measurements

Mice were fasted for 3 hr and serum insulin levels were measured by ELISA (Millipore) and blood glucose levels were measured with a One Touch Ultra 2 glucometer (Lifescan). For glucose tolerance test (GTT), mice were fasted for 16 hr, injected with 1 g/kg glucose, and blood was collected at several time points for the measurement of glucose and insulin levels. For insulin tolerance test (ITT), mice were fasted for 6 hr, injected with 0.5 mU/g insulin, and blood was collected at several time points for the measurement of glucose.

Adipose Tissue Measurements

Epididymal fat was stained with antibodies against murine MAC2 (Cedarlane) and PLIN2 (Abcam), and fluorescence images were acquired using an Olympus IX81 inverted wide field microscope. The number of crown-like structures in epididymal fat was by counting the number of adipocytes surrounded by MAC-2 positive signal per unit area. Between 4 and 6 mice were used per condition and 3 and 5 images were used per mouse. Epididymal fat caspase-3 activity was measured using the Apo-ONE kit (Promega) according to the manufacturer's protocol.

Liver Measurements

Livers were perfused with 30 mL of PBS before excision, homogenized, and TGs were measured using a TG quantification kit (Abcam) according to the manufacturer's protocol.

Statistics

Statistical significance was assessed using an unpaired, two-tailed, Student's t test. Replicate numbers for each experiment are indicated in the figure legends.

SUPPLEMENTAL INFORMATION

Supplemental Information includes Supplemental Experimental Procedures, seven figures, and one table and can be found with this article online at http://dx.doi.org/10.1016/j.celrep.2017.08.096.

AUTHOR CONTRIBUTIONS

Conceptualization, all authors; Investigation, B.R.C., K.Q.S., V.C.B.-L., G.Z., E.P., A.H., S.F., L.Z., B.A.H., A.S.H., and C.C.; Writing – Original Draft, L.B.; Writing – Reviewing & Editing, all authors; Supervision, L.B. and F.R.M.; Funding Acquisition, L.B. and F.R.M.

ACKNOWLEDGMENTS

This research was supported by grants from the NIH (R01DK102960 to L.B.; R37DK27083 to F.R.M.; R01HL093324 to F.R.M.; R01DK055267 to C.J.R.; P30 DK020595 to the DRTC Cell Biology Core, University of Chicago; T32DK087703 as support for B.R.C. and S.F.; and T32DK007074 as support for A.H.), the Bernice Goldblatt Endowment Fellowship, the University of Chicago (as support for C.C.), and the American Heart Association (10SDG3600027 to L.B.).

Received: June 1, 2017
Revised: July 25, 2017
Accepted: August 29, 2017
Published: September 26, 2017

REFERENCES

Akira, S., Takeda, K., and Kaisho, T. (2001). Toll-like receptors: critical proteins linking innate and acquired immunity. Nat. Immunol. *2*, 675–680.

Becker, L., Liu, N.C., Averill, M.M., Yuan, W., Pamir, N., Peng, Y., Irwin, A.D., Fu, X., Bornfeldt, K.E., and Heinecke, J.W. (2012). Unique proteomic signatures distinguish macrophages and dendritic cells. PLoS ONE *7*, e33297.

Bedard, K., and Krause, K.H. (2007). The NOX family of ROS-generating NADPH oxidases: physiology and pathophysiology. Physiol. Rev. *87*, 245–313.

Chawla, A., Nguyen, K.D., and Goh, Y.P. (2011). Macrophage-mediated inflammation in metabolic disease. Nat. Rev. Immunol. *11*, 738–749.

Clausen, B.E., Burkhardt, C., Reith, W., Renkawitz, R., and Förster, I. (1999). Conditional gene targeting in macrophages and granulocytes using LysMcre mice. Transgenic Res. *8*, 265–277.

Cohen, J.C., Horton, J.D., and Hobbs, H.H. (2011). Human fatty liver disease: old questions and new insights. Science *332*, 1519–1523.

Costford, S.R., Castro-Alves, J., Chan, K.L., Bailey, L.J., Woo, M., Belsham, D.D., Brumell, J.H., and Klip, A. (2014). Mice lacking NOX2 are hyperphagic and store fat preferentially in the liver. Am. J. Physiol. Endocrinol. Metab. *306*, E1341–E1353.

Fadok, V.A., Bratton, D.L., Konowal, A., Freed, P.W., Westcott, J.Y., and Henson, P.M. (1998). Macrophages that have ingested apoptotic cells in vitro inhibit proinflammatory cytokine production through autocrine/paracrine mechanisms involving TGF-beta, PGE2, and PAF. J. Clin. Invest. *101*, 890–898.

Fiorenza, C.G., Chou, S.H., and Mantzoros, C.S. (2011). Lipodystrophy: pathophysiology and advances in treatment. Nat. Rev. Endocrinol. *7*, 137–150.

Fitzgibbons, T.P., and Czech, M.P. (2016). Emerging evidence for beneficial macrophage functions in atherosclerosis and obesity-induced insulin resistance. J. Mol. Med. (Berl.) *94*, 267–275.

Gordon, S., and Taylor, P.R. (2005). Monocyte and macrophage heterogeneity. Nat. Rev. Immunol. *5*, 953–964.

Haka, A.S., Barbosa-Lorenzi, V.C., Lee, H.J., Falcone, D.J., Hudis, C.A., Dannenberg, A.J., and Maxfield, F.R. (2016). Exocytosis of macrophage lysosomes leads to digestion of apoptotic adipocytes and foam cell formation. J. Lipid Res. *57*, 980–992.

Han, M.S., Jung, D.Y., Morel, C., Lakhani, S.A., Kim, J.K., Flavell, R.A., and Davis, R.J. (2013). JNK expression by macrophages promotes obesity-induced insulin resistance and inflammation. Science *339*, 218–222.

Heinecke, N.L., Pratt, B.S., Vaisar, T., and Becker, L. (2010). PepC: proteomics software for identifying differentially expressed proteins based on spectral counting. Bioinformatics *26*, 1574–1575.

Hotamisligil, G.S., Shargill, N.S., and Spiegelman, B.M. (1993). Adipose expression of tumor necrosis factor-alpha: direct role in obesity-linked insulin resistance. Science *259*, 87–91.

Kratz, M., Coats, B.R., Hisert, K.B., Hagman, D., Mutskov, V., Peris, E., Schoenfelt, K.Q., Kuzma, J.N., Larson, I., Billing, P.S., et al. (2014). Metabolic dysfunction drives a mechanistically distinct proinflammatory phenotype in adipose tissue macrophages. Cell Metab. *20*, 614–625.

Lumeng, C.N., Deyoung, S.M., Bodzin, J.L., and Saltiel, A.R. (2007). Increased inflammatory properties of adipose tissue macrophages recruited during diet-induced obesity. Diabetes *56*, 16–23.

Murano, I., Barbatelli, G., Parisani, V., Latini, C., Muzzonigro, G., Castellucci, M., and Cinti, S. (2008). Dead adipocytes, detected as crown-like structures, are prevalent in visceral fat depots of genetically obese mice. J. Lipid Res. *49*, 1562–1568.

Nicholson, D.W., Ali, A., Thornberry, N.A., Vaillancourt, J.P., Ding, C.K., Gallant, M., Gareau, Y., Griffin, P.R., Labelle, M., Lazebnik, Y.A., et al. (1995). Identification and inhibition of the ICE/CED-3 protease necessary for mammalian apoptosis. Nature *376*, 37–43.

Odegaard, J.I., Ricardo-Gonzalez, R.R., Goforth, M.H., Morel, C.R., Subramanian, V., Mukundan, L., Red Eagle, A., Vats, D., Brombacher, F., Ferrante,

A.W., and Chawla, A. (2007). Macrophage-specific PPARgamma controls alternative activation and improves insulin resistance. Nature *447*, 1116–1120.

Olefsky, J.M., and Glass, C.K. (2010). Macrophages, inflammation, and insulin resistance. Annu. Rev. Physiol. *72*, 219–246.

Patsouris, D., Li, P.P., Thapar, D., Chapman, J., Olefsky, J.M., and Neels, J.G. (2008). Ablation of CD11c-positive cells normalizes insulin sensitivity in obese insulin resistant animals. Cell Metab. *8*, 301–309.

Pepping, J.K., Freeman, L.R., Gupta, S., Keller, J.N., and Bruce-Keller, A.J. (2013). NOX2 deficiency attenuates markers of adiposopathy and brain injury induced by high-fat diet. Am. J. Physiol. Endocrinol. Metab. *304*, E392–E404.

Robblee, M.M., Kim, C.C., Porter Abate, J., Valdearcos, M., Sandlund, K.L., Shenoy, M.K., Volmer, R., Iwawaki, T., and Koliwad, S.K. (2016). Saturated fatty acids engage an IRE1α-dependent pathway to activate the NLRP3 inflammasome in myeloid cells. Cell Rep. *14*, 2611–2623.

Rodríguez, A., Webster, P., Ortego, J., and Andrews, N.W. (1997). Lysosomes behave as Ca2+-regulated exocytic vesicles in fibroblasts and epithelial cells. J. Cell Biol. *137*, 93–104.

Saberi, M., Woods, N.B., de Luca, C., Schenk, S., Lu, J.C., Bandyopadhyay, G., Verma, I.M., and Olefsky, J.M. (2009). Hematopoietic cell-specific deletion of toll-like receptor 4 ameliorates hepatic and adipose tissue insulin resistance in high-fat-fed mice. Cell Metab. *10*, 419–429.

Sag, C.M., Schnelle, M., Zhang, J., Murdoch, C.E., Kossmann, S., Protti, A., Santos, C.X.C., Sawyer, G., Zhang, X., Mongue-Din, H., et al. (2017). Distinct regulatory effects of myeloid cell and endothelial cell NAPDH oxidase 2 on blood pressure. Circulation *135*, 2163–2177.

Seimon, T.A., Nadolski, M.J., Liao, X., Magallon, J., Nguyen, M., Feric, N.T., Koschinsky, M.L., Harkewicz, R., Witztum, J.L., Tsimikas, S., et al. (2010). Atherogenic lipids and lipoproteins trigger CD36-TLR2-dependent apoptosis in macrophages undergoing endoplasmic reticulum stress. Cell Metab. *12*, 467–482.

Shaul, M.E., Bennett, G., Strissel, K.J., Greenberg, A.S., and Obin, M.S. (2010). Dynamic, M2-like remodeling phenotypes of CD11c+ adipose tissue macrophages during high-fat diet-induced obesity in mice. Diabetes *59*, 1171–1181.

Shulman, G.I. (2014). Ectopic fat in insulin resistance, dyslipidemia, and cardiometabolic disease. N. Engl. J. Med. *371*, 1131–1141.

Strissel, K.J., Stancheva, Z., Miyoshi, H., Perfield, J.W., 2nd, DeFuria, J., Jick, Z., Greenberg, A.S., and Obin, M.S. (2007). Adipocyte death, adipose tissue remodeling, and obesity complications. Diabetes *56*, 2910–2918.

Sun, K., Kusminski, C.M., and Scherer, P.E. (2011). Adipose tissue remodeling and obesity. J. Clin. Invest. *121*, 2094–2101.

Talukdar, S., Oh, D.Y., Bandyopadhyay, G., Li, D., Xu, J., McNelis, J., Lu, M., Li, P., Yan, Q., Zhu, Y., et al. (2012). Neutrophils mediate insulin resistance in mice fed a high-fat diet through secreted elastase. Nat. Med. *18*, 1407–1412.

Tian, X.Y., Ganeshan, K., Hong, C., Nguyen, K.D., Qiu, Y., Kim, J., Tangirala, R.K., Tontonoz, P., and Chawla, A. (2016). Thermoneutral housing accelerates metabolic inflammation to potentiate atherosclerosis but not insulin resistance. Cell Metab. *23*, 165–178.

Wang, G.L., Jiang, B.H., Rue, E.A., and Semenza, G.L. (1995). Hypoxia-inducible factor 1 is a basic-helix-loop-helix-PAS heterodimer regulated by cellular O2 tension. Proc. Natl. Acad. Sci. USA *92*, 5510–5514.

Wei, X., Song, H., Yin, L., Rizzo, M.G., Sidhu, R., Covey, D.F., Ory, D.S., and Semenkovich, C.F. (2016). Fatty acid synthesis configures the plasma membrane for inflammation in diabetes. Nature *539*, 294–298.

Weisberg, S.P., McCann, D., Desai, M., Rosenbaum, M., Leibel, R.L., and Ferrante, A.W., Jr. (2003). Obesity is associated with macrophage accumulation in adipose tissue. J. Clin. Invest. *112*, 1796–1808.

Wernstedt Asterholm, I., Tao, C., Morley, T.S., Wang, Q.A., Delgado-Lopez, F., Wang, Z.V., and Scherer, P.E. (2014). Adipocyte inflammation is essential for healthy adipose tissue expansion and remodeling. Cell Metab. *20*, 103–118.

Xu, H., Barnes, G.T., Yang, Q., Tan, G., Yang, D., Chou, C.J., Sole, J., Nichols, A., Ross, J.S., Tartaglia, L.A., and Chen, H. (2003). Chronic inflammation in fat plays a crucial role in the development of obesity-related insulin resistance. J. Clin. Invest. *112*, 1821–1830.

Xu, X., Grijalva, A., Skowronski, A., van Eijk, M., Serlie, M.J., and Ferrante, A.W., Jr. (2013). Obesity activates a program of lysosomal-dependent lipid metabolism in adipose tissue macrophages independently of classic activation. Cell Metab. *18*, 816–830.